Title:

New insight in understanding the contribution of SGLT1 in cardiac glucose uptake: evidence for a truncated form in mice and humans

Authors:

Laura Ferté[1], Alice Marino[1], Sylvain Battault[1], Laurent Bultot[1], Anne Van Steenbergen[1], Anne Bol[2], Julien Cumps[1], Audrey Ginion[1], Hermann Koepsell[3], Laure Dumoutier[4], Louis Hue[1,5], Sandrine Horman[1], Luc Bertrand[1] and Christophe Beauloye[1,6]

Affiliations:

[1]Pôle de Recherche Cardiovasculaire, Institut de Recherche Expérimentale et Clinique, Université catholique de Louvain, Brussels, Belgium

[2]Center of Molecular Imaging, Radiotherapy and Oncology, Institut de Recherche Expérimentale et Clinique, Université catholique de Louvain, Brussels, Belgium

[3]Department of Molecular Plant Physiology and Biophysics, Julius von Sachs Institute, University of Würzburg, Würzburg, Germany

[4]Médecine Expérimentale, Institut de Duve, Université catholique de Louvain, Brussels, Belgium

[5]Institut de Duve, Université catholique de Louvain, Brussels, Belgium

[6]Division of Cardiology, Cliniques Universitaires Saint-Luc, Université catholique de Louvain, Brussels, Belgium

Running title:

Role of SGLT1 in cardiac glucose transport

Address for Correspondence:

Professor Christophe Beauloye, MD, PhD

Pôle de Recherche Cardiovasculaire

25 Institut de Recherche Expérimentale et Clinique, UCLouvain, Brussels, Belgium

26 55, Avenue Hippocrate B1.55.03.1322, BE-1200, Brussels, Belgium

27 Phone: +32 2 764 2750

28 Email: christophe.beauloye@uclouvain.be

Abstract

Although sodium-glucose co-transporter 1 (SGLT1) has been identified as one of the major SGLT isoforms expressed in the heart, its exact role remains elusive. Evidences using phlorizin, the most common inhibitor of SGLTs, suggested its role in glucose transport. However, phlorizin could also affect classical facilitated diffusion via glucose transporters (GLUTs), bringing into question the relevance of SGLT1 in overall cardiac glucose uptake. Accordingly, we assessed the contribution of SGLT1 in cardiac glucose uptake using the SGLT1 knock-out mouse model, which lacks exon 1. Glucose uptake was similar in cardiomyocytes isolated from SGLT1 knock-out ($^{\Delta ex1}$KO) and control littermate (WT) mice, either under basal state, insulin, or hyperglycemia. Similarly, *in vivo* basal and insulin-stimulated cardiac glucose transport measured by micro-PET scan technology did not differ between WT and $^{\Delta ex1}$KO mice. Micromolar concentrations of phlorizin had no impact on glucose uptake in either isolated WT or $^{\Delta ex1}$KO-derived cardiomyocytes. However, higher concentrations (1mM) completely inhibited insulin-stimulated glucose transport without affecting insulin signaling nor GLUT4 translocation, independently from cardiomyocyte genotype. Interestingly, we discover that mouse and human hearts expressed a shorter *slc5a1* transcript, leading to SGLT1 protein lacking transmembrane domains and residues involved in glucose and sodium bindings.

In conclusion, cardiac SGLT1 does not contribute to overall glucose uptake, probably due to the expression of *slc5a1* transcript variant. The inhibitory effect of phlorizin on cardiac glucose uptake is SGLT1-independent and can be explained by GLUT transporter inhibition. These data open new perspectives in understanding the role of SGLT1 in the heart.

New & noteworthy: Since the discovery of its expression in the heart, SGLT1 has been considered as similar as the intestine and a potential contributor to cardiac glucose transport. For the first time, we have demonstrated that a *slc5a1* transcript variant is present in the heart that has no significant impact on cardiac glucose handling.

Keywords: SGLT1, myocardium, glucose uptake, phlorizin, *slc5a1* variant

Introduction

To sustain its incessant work, the heart requires a constant supply of various metabolic substrates. Although it is widely known that fatty acids constitute the primary substrates for the heart, cardiac metabolism reliance on glucose becomes crucial in response to insulin, during ischemia, or in hypertrophic hearts. As glucose is hydrophilic, it needs transporters to cross the lipophilic membrane and enter into cells. Cardiac glucose uptake is usually thought to be mediated exclusively by facilitated glucose transporters (GLUTs) (*slc2* gene family). GLUT1 and GLUT4 are the two major isoforms expressed in the heart (1). GLUT1 is highly expressed in fetal hearts and declines after birth; it mainly mediates basal glucose uptake. Meanwhile, GLUT4 is more expressed in adult hearts and can be translocated to plasma membrane to favor glucose transport under certain stimuli, *i.e.*, insulin or ischemia (1).

In addition to GLUT transporters, a second family of glucose transporters, namely sodium-glucose co-transporters (SGLTs) (*slc5* gene family), has been described. These transporters rely on sodium gradient to bring sugar into cells (55). The SGLT family comprises seven isoforms: SGLT1, SGLT2, SGLT3, SGLT4, SGLT5, SGLT6 (SMIT2), and SMIT1 (55). These isoforms differ in substrate specificity, but they all transport glucose with different affinities. SGLT1 exhibits the highest affinity for glucose (K_m~0.5mM) among all SGLT isoforms (55). It is abundantly expressed in small intestine and kidneys, where it is responsible for glucose absorption and reabsorption, respectively (55). A high expression of SGLT1 along with SMIT1 has been demonstrated in human, rat, and murine hearts (3, 24, 47).

In humans, two transcript variants of *SLC5A1* (SGLT1) have been described, variant A and variant B (National Center for Biotechnology Information, NCBI; NM_000343.4 and NM_001256314.2, respectively). These variants differ in their 5' extremity. Variant A contains 15 exons, while variant B only has 14 exons and their sequences present 98% of

identity. Variant A encodes a 664 amino acid protein while variant B codes for a shorter protein of 537 amino acids lacking the first three transmembrane domains (9, 38, 55). In mice, such transcript variants have never been described. Murine *slc5a1* transcript encodes a 15 exon long mRNA producing a 666 amino acid protein (45).

Several lines of evidence suggest that SGLT1 could participate in cardiac glucose handling, mainly based on data showing that phlorizin, a SGLT inhibitor, reduces cardiomyocyte glucose uptake (3). However, to date, no studies have confirmed this hypothesis by means of genetic invalidation tools.

Here, we have demonstrated that the SGLT1 $^{\Delta ex1}$KO murine model does not exhibit significant difference in cardiac glucose transport *in vitro* and *in vivo*. Moreover, we have revealed that phlorizin, the most common SGLT inhibitor, can inhibit glucose transport independently of SGLT1 when used at an elevated but commonly employed concentration. Furthermore, for the first time, we demonstrated the existence of *slc5a1* transcript variants both in mouse and human hearts, probably resulting in SGLT1 truncated proteins.

Material and methods

Animal handling

Animal handling was approved by local authorities (*Comité d'éthique facultaire pour l'expérimentation animale*, 2016/UCL/MD/027) and performed in agreement with guidelines on animal experimentation at our institution. This study conformed to the *Guide for the Care and Use of Laboratory Animals* published by the US National Institutes of Health (NIH Publication No. 85-23, revised 1996). SGLT1-deficient mice were generated as described elsewhere (19). Koepsell's group performed genetic manipulations that lead to a deletion of exon 1 and part of the promoter from *slc5a1* murine gene (19). In this paper, these mice and their control littermates are called SGLT1 $^{\Delta ex1}$KO and WT, respectively. SGLT1 $^{\Delta ex1}$KO animals die shortly after weaning from glucose/galactose malabsorption syndrome (19). To avoid the development of this syndrome, the $^{\Delta ex1}$KO mice were fed using a glucose-/galactose-free diet. WT littermate group fed with a glucose-/galactose-free diet was used as control.

Isolation and culture of mouse and rat cardiomyocytes

Adult mouse cardiomyocytes were isolated from SGLT1 breeding lineage and C57Bl/6N mice and cultured as described previously (2). Briefly, two- to four-month-old mice were anesthetized using a mixture of xylazine (10mg/kg) and ketamine (80mg/kg). Once asleep, mice were dislocated, and the heart was immediately excised. Hearts were then perfused for 6 minutes and subsequently digested with Liberase DH enzyme (0.020mg/heart, Roche 0501054001) and trypsin (2.1mg/heart, Life Technologies 15090-046) for another 25 minutes. Cells were purified, cultured, and plated on laminin-coated dishes and incubated for one hour in fresh minimum essential medium (MEM) with Hank's salts (Life Technologies 11575–032) supplemented with L-glutamine (2mM), bovine serum albumin (BSA; 100µg/mL),

penicillin (100U/mL), and streptomycin (100µg/mL). Treatment details are provided in figure legends.

Rat adult cardiomyocytes were isolated and cultured, as described previously (7). Briefly, hearts from 250g male Wistar rats were excised and retrogradely perfused via the aorta. After 10 minutes of perfusion with Ca^{2+}-free Krebs-Henseleit buffer containing 5mM glucose, 2mM pyruvate, and 10mM HEPES (pH 7.4), hearts were digested by adding 0.2mM Ca^{2+}, 1mg/mL collagenase (Worthington), and 0.4% (wt/vol) BSA. Once digested, hearts were mechanically disrupted with scissors, and Ca^{2+} was added to reach a final concentration of 1mM. Finally, cardiomyocytes were purified and washed by sedimentation. Cells were cultured in Medium 199 (supplemented with 2mM carnitine, 5mM creatine, 5mM taurine, 10^{-10}M triiodothyronine, 0.2% free fatty acid BSA, and antibiotics) for one hour prior to treatment. Treatment details are provided in figure legends.

Glucose uptake in cultured mouse cardiomyocytes

Glucose uptake was measured, as described previously (7, 10), by following [2-^{3}H]-glucose detritiation rate, which occurs after glucose phosphorylation during rapid isomerization of hexose-6-phosphate catalyzed by phosphoglucose isomerase. Briefly, for the last 30 minutes of treatment, 0.2µCi/ml of [2-^{3}H]-glucose were added to the MEM culture medium containing 5.5mM of glucose. Tritiated water present in the supernatant was separated from tritiated glucose using chromatography on anion exchange resin (borate form) and measured by a scintillation counter.

When specified, glucose uptake was additionally measured by the entry of [^{3}H]-2-deoxyglucose. Once within the cells, [^{3}H]-2-deoxyglucose was phosphorylated by hexokinase and could not be further metabolized. After washing the cells, the phosphorylated form of

144 [^{3}H]-2-deoxyglucose trapped within the cell was released by cellular lysis and measured using
145 a scintillation counter.

146 **Glycogen content measurement**

147 Glycogen content was measured following the protocol described in Passonneau and
148 Lauderdale, 1974 (34). Hearts from two- to four-month-old fed mice were excised and rapidly
149 snap frozen. The frozen hearts were homogenized in 10 volume (vol/wt) of 1M KOH and
150 extracted using an Ultra-Thurax. Samples were incubated at 80°C for 15 minutes to complete
151 the extraction and then neutralized with 3.3M acetic acid. Supernatant obtained after
152 centrifugation (6,000 rpm for six minutes) was employed for the assay. Glycogen was
153 converted to glucose via the enzyme amylo-α-1,4-α-1,6-glucosidase. Glycogen content assay
154 was based on quantifying the NADPH content obtained from the NADP conversion during
155 production of 6-phosphogluconic acid from glucose-6-phosphate by the glucose-6-phosphate
156 dehydrogenase enzyme. Glucose-6-phosphate was obtained from glucose by adding the
157 hexokinase enzyme. Absorbance of samples was measured at three different time points:
158 sample and buffer for background absorbance (E0), after adding glucose-6-phosphate
159 dehydrogenase to measure glucose-6-phosphate from sources other than glycogen (E1), and
160 after adding ATP-$MgCl_2$ and hexokinase (E2). Glycogen content was calculated by
161 subtracting E1 and blank from E2. Results were expressed as µmol/mg of frozen tissue.

162 **RNA extraction, RT-qPCR and RT-PCR analysis**

163 Total mRNA was extracted from whole hearts from SGLT1 WT and $^{\Delta ex1}$KO or C57BL/6N
164 cardiomyocytes via a chloroform/isopropanol procedure (Tripure Isolation Reagent, Roche
165 11667165001) and subjected to on-column treatment using an RNAse-free DNase set (Qiagen
166 79254). RNA content was quantified using a nanodrop (Thermo Scientific); 1µg of each RNA
167 preparation was submitted to reverse transcription (RT) for 5 minutes at 35°C followed by 30

minutes at 42°C and 5 minutes at 85°C using an iScript™ cDNA synthesis kit (Bio-Rad laboratories 1708891). All PCRs contained 2µl of RT reaction diluted 5 times and 0.25µM of forward and reverse primers in 25µl volume. PCR was performed with GoTaq G2 DNA polymerase (Promega M7845), and reactions were heated to 95 °C for 2 min, followed by 45 cycles of 95 °C for 30 s, 59–60 °C for 30 s, 72 °C for 1-2 min and then heated at 72 °C for 5 additional min in a MJ MiniTM Gradient Thermal Cycler (Biorad PTC-1148). The PCR products were separated by agarose gel electrophoresis (1 to 2% wt/v) and stained with ethidium bromide. Primer sequences are listed in supplementary table 1 (dx.doi.org/10.17504/protocols.io.bqr6mv9e). qRT-PCR was performed with a CFX Connect™ Real-Time PCR detection system (Bio-Rad) using qPCR core kit for SYBR green (Eurogentec). The mRNA level of each gene was normalized to the housekeeping gene ribosomal protein L32 after ΔΔCt correction. Primer sequences are listed in supplementary table 2 (dx.doi.org/10.17504/protocols.io.bqr6mv9e).

Evaluation of GLUT4 translocation

Once plated on six-well plates, rat adult cardiomyocytes were infected with adenoviruses expressing a GFP-modified GLUT4 protein tagged with an HA-tag at the NH_2-terminal part (extracellular part when translocated) (HA-GLUT4-GFP), as previously described (37). Then, 48 hours after infection, phlorizin (to reach a final concentration of 1mM) was added 15 minutes prior to insulin stimulation, which lasted for 30 additional minutes. Cells were then fixed using 4% paraformaldehyde and blocked for 30 minutes with PBS/BSA 5%. Primary antibody (HA-Tag (C29F4) Rabbit mAb, Cell Signaling) and secondary antibody (Alexa Fluor 568 donkey anti-rabbit IgG (H+L), Invitrogen), both dissolved in PBS/BSA 1%, were incubated on the cells for one hour each before mounting on slides. Staining and GFP fluorescence were visualized under a Zeiss Imager.Z1 microscope equipped with an ApoTome device. Red fluorescent dots (HA staining reflecting GLUT4 attached to the

membrane) were quantified relative to GFP (total GLUT4 protein) by means of Image J software.

Immunoblotting analysis

Protein content was measured via Bradford method with BSA as standard. Immunoblotting was performed with extracts separated on 8% or 10% SDS-PAGE, transferred to polyvinylidene difluoride membranes that were blocked with BSA 5%, then incubated with corresponding antibodies. Following incubation with an appropriate secondary antibody (anti-rabbit or anti-mouse), proteins were visualized using electrochemical luminescence (Pierce). GLUT detection was performed on whole-heart protein extract; eEF2 served as a loading control when investigating GLUT1, GLUT4, and S6 expression and phosphorylation state, while GAPDH or eEF2 was employed as a loading control when investigating AKT expression and phosphorylation. Primary antibodies used are listed in Supplementary Table 3 (dx.doi.org/10.17504/protocols.io.bqr6mv9e).

Glucose uptake in entire animals using PET/CT imaging

In vivo cardiac glucose uptake was assessed using whole-body PET imaging performed on a dedicated small-animal PET scanner (Mosaic, Philips Medical Systems) with a spatial resolution of 2.7mm (FWHM) (22). Prior to treatment, mice underwent overnight fasting. Animals were injected with insulin (0.5U/kg) five minutes prior to a 2-deoxy-2-[^{18}F]-D-glucose (^{18}F-FDG) injection at a dose of 6.7–12MBq/animal (Betaplus Pharma). For phlorizin treatment, 400mg/kg (dissolved in 75% saline, 15% DMSO, and 10% ethanol) or vehicle was injected 30 minutes prior to insulin stimulation. All injections were performed intraperitoneally. Animals were kept under a heating lamp during the one-hour ^{18}F-FDG uptake. Thereafter, they were anesthetized with 2% isoflurane in air at 2L/min and placed on a heated animal bed, which provided anesthesia through a nose cone. A 10-minute emission

scan was performed one hour after tracer injection and immediately followed by a 10-minute transmission scan using a 370MBq ^{137}Cs source. Anesthetized mice were then transferred on the same bed to a micro-CT (NanoSPECT/CT Small Animal Imager, Bioscan Inc.) for anatomical reference image acquisition. After correction for attenuation factors obtained from the transmission scan, PET images were reconstructed using a fully three-dimensional interactive algorithm (3D-RAMLA) in a 128 x 128 x 120 matrix, with a voxel of 1mm^3. Regions of interest were delineated on the reconstructed PET images using the PMOD software (PMOD^{TM}, version 3.406, PMOD Technologies Ltd, Zurich, Switzerland). To discriminate hot pixels from neighboring tissues, PET/CT fused images were employed. Cardiac tracer uptake was assessed and expressed as standardized uptake value (SUV) max (normalized to body weight).

RNA sequencing and human biopsies

RNA sequencing (RNA seq) data used for mouse study have been obtained using other breeding lineages, SMIT1 WT and KO, available in our animal facility and described elsewhere (6). RNA seq data were aligned with SGLT1 mRNA sequence (NCBI RefSeq NM_019810.4) from mus musculus. For human data, we used 3 publicly available studies found in GEO accession database GSE116250 (44), GSE126569 (42) and GSE123976 (35). From these studies, control or non-failing heart data were aligned to variant A (NCBI RefSeq NM_000343.4) or variant B (NCBI RefSeq NM_001256314.2) SGLT1 mRNA sequences in nucleotide BLAST from NCBI.

Human heart tissues for PCR results were obtained from patients undergoing left ventricular assist device implantation as described previously (47). This protocol was approved by the local ethic committee (Comité éthique hospitalo-facultaire des Cliniques Universitaires St. Luc, Brussels, Belgium). All experimental procedures were performed in accordance with

241 relevant guidelines and regulations. Intestine samples, used as positive controls, were residual
242 material from surgery.

243 **Statistical analysis**

244 All data were expressed as means ± SEM. Statistical analyses were performed by a two-way
245 ANOVA test followed by Sidak's multiple comparison post-hoc test for multiple group
246 comparisons. Comparison of two groups was performed using an unpaired Student's t-test.
247 Statistical significance was considered when p-value was less than 0.05. All analyses were
248 performed using GraphPad Prism (GraphPad Software).

Results

Cardiac glucose uptake in isolated cardiomyocytes from SGLT1 $^{\Delta ex1}$KO mice.

As introduced earlier, numerous studies have advocated a role of SGLT1 in cardiac glucose uptake (3, 4, 23, 24, 57). Therefore, we studied this process in a SGLT1 knock-out mouse model generated by Koepsell group. This KO has been produced by deleting exon 1 (reason why we called it SGLT1 $^{\Delta ex1}$KO) and previously used for studies in various tissues, including the heart (19, 29). We first examined the contribution of SGLT1 in glucose uptake in isolated murine cardiomyocytes in culture by measuring the intracellular accumulation of [^{3}H]-2-deoxyglucose (2DG). 2DG uptake did not differ between cardiomyocytes from SGLT1 WT and $^{\Delta ex1}$KO mice under normoglycemia (NG; 5mM) (Fig. 1A). As previously described (43, 60), basal 2DG uptake was largely increased in the presence of hyperglycemia (HG, 21mM, three-fold) or 3nM insulin (two-fold) in WT cardiomyocytes. 2DG uptake stimulation was similar in $^{\Delta ex1}$KO cardiomyocytes (Fig. 1A).

Although radiolabeled 2DG is employed to measure glucose uptake, electrophysiological studies have demonstrated that 2DG is a poor substrate for SGLT transporters (25, 33, 56, 58). Thus, uptake measured using this approach primarily represents glucose transport through GLUT transporters, but not SGLT1. Therefore, we employed a [2-^{3}H]-glucose radiotracer to evaluate SGLT1-dependent glucose uptake. Similarly to 2DG, SGLT1 WT and $^{\Delta ex1}$KO cardiomyocytes exhibited same level of [2-^{3}H]-glucose uptake under basal conditions, as well as under HG or insulin (Fig. 1B).

It has recently been hypothesized that SGLT1 participates to ischemia-induced glucose utilization via the activation of AMP-activated protein kinase (AMPK); such a mechanism is proposed as a major process responsible for ischemic preconditioning-induced cardioprotection (27). Therefore, we evaluated the role of SGLT1 on glucose uptake

following oligomycin-induced AMPK activation. Oligomycin, like ischemia, increases the AMP/ATP ratio, promoting AMPK activation and glucose uptake independently of insulin (7, 37). A five-fold increase in glucose uptake into WT cardiomyocytes was observed one hour after adding 1μM oligomycin (Fig. 1C). As observed with insulin and HG, these responses were not different in $^{\Delta ex1}$KO cardiomyocytes (Fig. 1C), indicating that SGLT1 does not contribute to cardiac AMPK-induced glucose uptake.

In vivo glucose uptake and glycogen content in SGLT1 $^{\Delta ex1}$KO mice.

Contribution of SGLT1 to cardiac glucose uptake was further investigated *in vivo* on anesthetized animals via a micro-PET scan using radiotracer ^{18}F-FDG, as previously described (16, 54). Maximal standard uptake values (SUV_{max}) values in hearts of SGLT1 WT and $^{\Delta ex1}$KO mice were similar in basal (0.72 ± 0.18 vs. 0.67 ± 0.12, respectively) and insulin-stimulated states (2.76 ± 0.68 vs. 2.62 ± 0.22, respectively) (Fig. 1D). As glucose transport, glycogen content, the main form of glucose storage, did not differ between SGLT1 $^{\Delta ex1}$KO and WT mice (Fig. 1E). In agreement with our *in vitro* experiments, these *in vivo* observations do not support a major role of SGLT1 in cardiac glucose handling.

GLUT transporters in SGLT1 $^{\Delta ex1}$KO mice.

Lack of SGLT1's effect on glucose transport could be due to a compensatory mechanism favoring facilitated glucose uptake in absence of SGLT1. To test this hypothesis, we analyzed GLUT transporters at three levels: expression, activity, and regulation. Initial analysis of cardiac GLUT1 and GLUT4 expression at the mRNA and protein levels revealed no significant differences between SGLT1 WT and $^{\Delta ex1}$KO mice (Fig. 2A–D). Then, we investigated the contribution of GLUT4 to glucose uptake in SGLT1 WT and $^{\Delta ex1}$KO cardiomyocytes. To abolish GLUT4 contribution, we measured insulin- and oligomycin-stimulated [2-^{3}H]-glucose uptake in presence of indinavir, a specific GLUT4 inhibitor (31).

297 Insulin- and oligomycin-stimulated glucose uptake are primarily due to recruitment of
298 GLUT4 to plasma membrane (18, 37, 39). An excess of GLUT4 translocation could
299 potentially mask SGLT1 contribution in glucose uptake. Under basal conditions, treatment
300 with 50μM indinavir had no effect either on SGLT1 WT or $^{\Delta ex1}$KO cardiomyocytes (Fig. 1C).
301 Moreover, insulin- and oligomycin-stimulated glucose uptakes were abolished to a similar
302 extent using indinavir in cardiomyocytes from both genotypes (Fig. 1C). These results
303 indicate that GLUT4 does not participate in compensatory glucose uptake in SGLT1 $^{\Delta ex1}$KO
304 cardiomyocytes.
305 Finally, SGLT1 could influence signaling pathways controlling GLUT4 translocation and,
306 particularly, insulin and AMPK signaling pathways. To test this hypothesis, we analyzed
307 phosphorylation of two downstream insulin signaling targets, namely Akt/PKB and S6. We
308 observed no difference in Akt/PKB and S6 phosphorylation under basal, HG, or insulin
309 conditions in either SGLT1 $^{\Delta ex1}$KO or WT cardiomyocytes (Fig. 2E-F). In addition, we
310 assessed the impact of SGLT1 on AMPK activation following oligomycin stimulation.
311 Immunoblotting for phospho-AMPK did not exhibit any changes in AMPK activation in
312 cardiomyocytes isolated from SGLT1 $^{\Delta ex1}$KO mice compared to WT cardiomyocytes (Fig.
313 2G). Altogether, these results suggest that there is no compensation by GLUT expression,
314 function, or regulation in SGLT1 $^{\Delta ex1}$KO mice.

315 **Impact of phlorizin on glucose uptake in SGLT1 $^{\Delta ex1}$KO mice.**

316 The role of cardiac SGLT1 in physiological and pathological conditions has been investigated
317 using phlorizin. However, concerns remain with respect to potential phlorizin off-target
318 effects on GLUT-dependent sugar transport. To address this issue, we first evaluated the
319 impact of increasing phlorizin concentrations on glucose uptake in isolated mouse
320 cardiomyocytes; 10μM and 100μM phlorizin scarcely affected basal cardiomyocyte [2-^{3}H]-
321 glucose uptake (Fig. 3A), whereas 1mM of phlorizin significantly reduced it. More

importantly, phlorizin inhibited insulin-stimulated cardiomyocyte glucose uptake in a dose-dependent fashion, with insulin response being blunted at 1mM (Fig. 3A). To evaluate the role of SGLT1 on phlorizin effects, these experiments were additionally conducted on SGLT1 $^{\Delta ex1}$KO cardiomyocytes. In both basal and insulin-stimulated states, phlorizin response was similar between the two genotypes (Fig. 3A). These results were confirmed *in vivo* by measuring cardiac ^{18}F-FDG uptake in SGLT1 WT and $^{\Delta ex1}$KO mice via a micro-PET scan. In presence of insulin stimulation, we observed an inhibition of cardiac glucose uptake from WT mice when a standard concentration (400mg/kg) of phlorizin was employed (Fig. 3B). Interestingly, this inhibitory effect of phlorizin on insulin-stimulated cardiac glucose transport was similarly present in SGLT1 $^{\Delta ex1}$KO mice (Fig. 3B). Two hours after insulin injection, glucose level in the blood was similar despite the genotype or phlorizin treatment, although hypoglycemia tended to be more pronounced in presence of phlorizin (Fig. 3B). It is worthy to notice that phlorizin treatment per se, induced a significant decrease in glycemia, which was identical in SGLT1 WT and $^{\Delta ex1}$KO animals (for SGLT1 WT: control, 141±5mg/dl without phlorizin; 81±4mg/dl with phlorizin, $p<0.05$; for SGLT1 $^{\Delta ex1}$KO: control, 121±8mg/dl without phlorizin; 71±7mg/dl with phlorizin, $p<0.05$).

Next, we ruled out the possibility that high phlorizin concentrations do block the insulin-signaling pathway or GLUT4 translocation to plasma membrane. We assessed the effect of 1mM phlorizin on insulin-induced Akt/PKB phosphorylation (on Ser473) and S6 phosphorylation in isolated mouse cardiomyocytes in culture and GLUT4 translocation using a model overexpressing HA-GLUT4-GFP fusion protein, as described previously (37). Rather than reduce it, phlorizin actually enhanced insulin-induced Akt/PKB and S6 phosphorylation (Fig. 4A–B). Moreover, phlorizin effect on insulin pathway was similar in SGLT1 $^{\Delta ex1}$KO cardiomyocytes (Fig. 4A–B). We also analyzed Akt/PKB phosphorylation *in vivo* on hearts from SGLT1 WT mice treated with phlorizin and/or insulin. In accordance to our *in vitro*

data, we showed no inhibition, and even a trend to an enhanced insulin signaling in presence of phlorizin (Fig. 4C). In agreement with Akt/PKB phosphorylation data, we observed that phlorizin tends to further favor GLUT4 translocation to plasma membrane in response to insulin (Fig. 5). Taken together, these results demonstrate that phlorizin directly interferes with GLUT activity so as to reduce glucose transport without affecting its translocation.

Based on these data, we assume that high phlorizin concentrations affect cardiac glucose transport through a mechanism that is unrelated to SGLT1.

Transcript variant of *slc5a1* in mouse hearts.

The lack of cardiac phenotype observed in SGLT1 $^{\Delta ex1}$KO mice, without any impact on cardiac glucose uptake, on cardiac glycogen content or on phlorizin inhibitory effect, could be considered as intriguing. Therefore, we further investigated SGLT1 expression in our experimental model. As expected (19), we confirmed the deletion of exon 1 and part of the promotor in heart genomic DNA (Fig. 6A). We next analyzed SGLT1 deletion at the mRNA level (Fig. 6B). As expected, the lack of exon 1 was confirmed in intestine SGLT1 mRNA in $^{\Delta ex1}$KO mice. By contrast to the intestine, no expression of exon 1-containing transcripts of *slc5a1* could be detected in SGLT1 WT and $^{\Delta ex1}$KO hearts (Fig. 6C). Puzzled by such results, we further characterized cardiac SGLT1 mRNA via a systematic PCR amplification of each exon. Interestingly, PCR results demonstrated the presence of a cardiac truncated SGLT1 mRNA containing exon 9 to exon 15 in both SGLT1 WT and $^{\Delta ex1}$KO hearts as well as C57BL/6N isolated cardiomyocytes (Fig. 6C-E and Supplementary Fig. 1, dx.doi.org/10.17504/protocols.io.bqr7mv9n). Those transcripts were quantified via qPCR showing no differences between WT and $^{\Delta ex1}$KO (data not shown).

With the help of RNA sequencing (RNA seq) data obtained from heart of control mice, we performed a coverage analysis of SGLT1 mRNA sequence. We found that cardiac SGLT1

mRNA expression was low since reads matching SGLT1 sequence were rare. Moreover, we observed reads covering SGLT1 mRNA sequence starting from approximately 1200bp, corresponding to exon 9 (Fig. 6F). These data confirmed the presence of a transcript variant for *slc5a1* in mouse hearts that lacks a large 5' portion (exons 1 to 8). To our knowledge, it is the first report of a transcript variant of *slc5a1* in murine heart.

Expression of variant B, the shortest *SLC5A1* transcript variant in human hearts.

Our discovery of a truncated SGLT1 mRNA in murine hearts questioned cardiac SGLT1 mRNA expression in other species, particularly in humans. As stated in the introduction section, two variants of *SLC5A1* have been detected in human tissues. Variant A was not expressed in the heart while variant B of *SLC5A1* could be detected and amplified (Fig. 7A-B). To confirm our results, we carried out an *in silico* analysis of RNA seq data from human hearts of three different studies that are publicly available in GEO accession database (35, 42, 44). RNA seq data were aligned with the known sequences of variant A or variant B. These alignments, as well as a representation of *SLC5A1* variants in human, are shown in Fig. 7C-D. We observed specific RNA seq reads for variant B and not for variant A (Fig 7C-D). Altogether, these data show for the first time that human heart expresses *SLC5A1* transcript variant B, encoding a shorter protein that loses three transmembrane domains as well as residues involved in glucose and sodium bindings. Further investigations are needed to understand the role and potential activity of this protein isoform in human heart.

Discussion

To date, no clear function of SGLT1 has been identified within the heart. Previous studies, including from our group have shown that SGLT1 and SMIT1 are expressed in human, mouse, and rat hearts (3, 24, 47). The main findings of this study are that no significant changes in murine cardiac glucose handling is observed in the classical genetic model of SGLT1 invalidation and that high phlorizin concentrations lower cardiac glucose uptake independently of SGLT1. Importantly, we showed that murine and human hearts express *slc5a1* alternative transcripts encoding for truncated proteins, unlikely to be involved in glucose transport (Fig. 8).

In contrast to GLUT-dependent facilitated glucose transport, SGLTs employ the sodium gradient maintained by the Na^+/K^+-ATPase (25, 55) to actively uptake glucose. SGLTs exist under several isoforms that all differ in their affinity towards glucose (Barbeau, #148) and alternative monosaccharides (30, 55). Several studies highlighted monosaccharide structural requirements, including a pyranose ring in D-configuration, to be transported through SGLTs. D-glucose is recognized by SGLTs through its C2-hydroxyl group and C5-methyl or substituted methyl group (13, 26, 52). Therefore, SGLT-dependent glucose transport theoretically cannot be estimated by measuring intracellular accumulation of radiolabeled glucose analogues, such as 2DG or 2FDG, because these tracers lack the structural specificities mentioned above. Thus, it is not surprising that no differences could be observed in 2DG or 2FDG uptake between SGLT1 WT and $^{\Delta ex1}$KO mice *in vitro* and *in vivo*. Furthermore, we obtained similar results with a [2-^{3}H]-glucose radiotracer transported by SGLTs, suggesting that SGLT1 contribution to cardiac glucose uptake is, at best, marginal. In addition, it should be noted that SGLT1 $^{\Delta ex1}$KO does not affect facilitated glucose transport.

When interpreting the passive or active nature of glucose transport, a warning applies to the specificity of inhibitors used to discriminate glucose transporters; typically phloretin (GLUT

inhibitor) and phlorizin (SGLT inhibitor). Phlorizin is considered a SGLT1 inhibitor, although it actually inhibits most SGLT isoforms with different affinities (K_i≈140nM for SGLT1, K_i≈11nM for SGLT2, K_i≈120µM for SGLT3, K_i≈10µM for SGLT4, K_i≈1.7µM for SGLT5, K_i≈76µM for SGLT6, K_i≈60µM for SMIT1) (12, 17, 20, 46, 50). Phlorizin barely affects glucose handling at concentrations close to its K_i for SGLT1. However, our data clearly indicate that 1mM of phlorizin can resume phloretin effects on glucose uptake and therefore behave as an inhibitor of facilitated transport. Moreover, our data using 2FDG in PET scan further confirm the indirect effect of 400mg/kg of phlorizin on GLUT transporters since SGLTs do not transport 2FDG. These essential results question the role of SGLT1 demonstrated via pharmacological approach with high phlorizin doses. Indeed, a previous study has shown that SGLT1 mediates insulin- and leptin-induced glucose uptake in mouse heart. The use of high *in vivo* concentrations of phlorizin (400mg/kg) and 2-deoxy-D-[^{14}C]-glucose as glucose tracer indicate that these results rather reflect an unspecific effect of phlorizin on GLUT transporters. As phlorizin differs from phloretin by its β-D-glucopyranosyl residue attached at position 2, along with a tendency to be hydrolyzed to its aglycone form (15), a high phlorizin concentration can alter facilitated transport, either directly or through its conversion into phloretin.

SGLT1 expression in mouse heart remains controversial. Of importance, we report, for the first time, the existence of a *slc5a1* transcript variant in mouse heart. Indeed, cardiac SGLT1 mRNA starts from exon 9 to exon 15, making it undetectable with primers targeting exons 1 to 8. One may wonder whether this particular expression could not be specific to our mouse breeding lineage. The absence of full length has been recapitulated in all strains that we have studied, ruling out such hypothesis. Our discovery explains apparent discrepancies regarding SGLT1 mRNA detection in the heart. Madunic-Vrhovac et al. have observed no cardiac SGLT1 mRNA (28) using primers amplifying exons 1 to 4 of *slc5a1* mRNA (28) although

most of other studies have used primers specific for the 3' extremity (3, 27, 29, 36), which is present in mouse heart. The *slc5a1* cardiac transcript variant is detectable in both WT and SGLT1 $^{\Delta ex1}$KO hearts. The expected mouse cardiac SGLT1 isoform is a shorter protein, lacking a large N-terminal extremity that contains residues involved in glucose and sodium bindings as well as 8 transmembrane domains (9, 38, 55), all required for glucose transport (Fig. 8A-B). Accordingly, a role of SGLT1 in cardiac glucose uptake is unlikely. In line with our data, a recent study involving transgenic mice with cardiomyocyte-specific RNA interference knockdown of SGLT1 (TG$^{SGLT1\text{-}DOWN}$) showed that SGLT1 reduction barely affects *ex vivo* cardiac glucose consumption, although glucose uptake was not directly measured using radioactive tracers (27). One may notice that the SGLT1 siRNA sequence they used targets the mouse cardiac variant of *slc5a1* and potentially knockdowns all putative cardiac SGLT1 proteins. Although there were no differences between the WT and $^{\Delta ex1}$KO in term of *slc5a1* transcript in the heart, we have several evidence still supporting the lack of SGLT1-dependent glucose transport. Indeed, both genotypes show (i) similar responses to different glucose tracers, (ii) similar impact of indinavir, and (iii) absence of key regions for glucose binding and transport in the sequence expressed in the heart.

Under basal state, SGLT1 $^{\Delta ex1}$KO and TG$^{SGLT1\text{-}DOWN}$ mice exhibit no specific cardiac phenotype (27, 47). However, a role of cardiac SGLT1 has been advocated in several pathological conditions. First, SGLT1 has been implicated in the pathophysiology of cardiomyopathy linked to *PRKAG2* (gene expressing AMPK regulatory subunit) mutation. It can mediate the increase in glycogen storage induced by the γ2 subunit mutation of AMPK. SGLT1 knockdown was shown to decrease cardiac glycogen content and improve cardiac function in a model of PRKAG2 cardiomyopathy (36). Second, SGLT1 absence has been shown to counteract transaortic constriction-induced cardiac hypertrophy, resulting in well-preserved left ventricular function under pressure overload (29). Finally, other lines of

466 evidence suggest a contribution of SGLT1 in cardiac ischemia-reperfusion injury. Indeed,
467 SGLT1 expression is increased following coronary ligation in mice (3, 27), and SGLT1
468 knockdown protects the heart from ischemia-reperfusion injury by reducing protein kinase C
469 (PKC), NADPH oxidase (NOX2) activation, and reactive oxygen species production (27).
470 These results seem to be in conflict with the observations of Kashiwagi et al. (24), who
471 showed that SGLT inhibition using phlorizin is deleterious upon ischemia-reperfusion. These
472 contradictory results could be explained by phlorizin concentrations used impacting GLUT-
473 mediated glucose uptake, indicating that phlorizin should be employed with caution. In all
474 these pathological situations, mechanisms beyond cardiac SGLT1 remain elusive and need
475 further investigation. One may hypothesize that cardiac SGLT1, even truncated, modifies
476 signaling pathways involved in pathophysiology.

477 Finally, our data also demonstrate the presence of an alternative transcript of *SLC5A1* in
478 human heart. Several studies have shown a significant cardiac expression of SGLT1 in human
479 (3, 14, 24, 48, 49, 51, 59) but we are the first to specify that transcript variant B is the one
480 expressed, at least in all analyzed samples, leading to the expression of a shorter protein
481 lacking residues implicated in glucose and sodium bindings as well as three transmembrane
482 domains (Fig. 8C). This cardio-specific variant of SGLT1 might exhibit impaired glucose
483 affinity, transport capacity as well as sensitivity to inhibitors, compared to other organs (9, 38,
484 55).

485 Interestingly, SGLT2 inhibitors, widely used for Type 2 diabetes mellitus treatment, have
486 shown cardioprotective properties independently of their blood glucose-lowering effect (32,
487 53, 61). However, several studies highlighted the lack of SGLT2 expression in the heart (14,
488 21, 47, 48, 51) questioning the possibility of an indirect effect of these inhibitors on cardiac
489 function. The beneficial cardiovascular effect of SGLT2 inhibitors is, therefore, intriguing and
490 currently being investigated (11). The affinity of these inhibitors for SGLT1 cardiac isoform

491 remains to be defined. Moreover, given SGLT1 functions in glucose renal reabsorption and
492 intestinal absorption (55), dual SGLT1/SGLT2 inhibitors have been recently developed in the
493 context of diabetes treatment (40, 41), which also conferred the ability to dramatically reduce
494 risk of cardiovascular death or hospitalization for heart failure in diabetic patients (8). Long-
495 term results will help determine the potential impact of SGLT1 inhibition on various organs in
496 which it is expressed, including the heart. Understanding the role of SGLT1 outside intestine
497 or kidney is of clinical relevance in this context (5).

498 Several limitations of our study have to be pointed out. While our cardiac glycogen
499 measurements showed no changes in SGLT1 WT and $^{\Delta ex1}$KO animals at the basal state, the
500 latter has not been verified in stimulated conditions and pathology. Moreover, technical issues
501 concerning GLUT4 translocation to the plasma membrane in SGLT1 $^{\Delta ex1}$KO model would
502 have to be addressed to rule out an effect of SGLT1 in this process. Further investigation will
503 be conducted to decipher SGLT1 implication in glycogen and glucose homeostasis in
504 stimulated states and pathology in the heart. Lastly, we were not able to assess the impact of
505 the cardiac SGLT1 mRNA variant on its protein expression due to the lack of specific
506 available antibodies. New tools and further investigations are needed to address SGLT1
507 protein expression in the heart, in an appropriate manner.

508 **Conclusion**

509 In this study, we have demonstrated that SGLT1 $^{\Delta ex1}$KO murine model exhibit normal glucose
510 handling and cardiac glucose transport in isolated cardiomyocytes or *in vivo.* This could be
511 explained by the expression of a SGLT1 mRNA lacking exons 1 to 8 leading to a truncated
512 protein in mouse hearts. A different *slc5a1* transcript variant is also expressed in human heart.
513 Further investigations are required to elucidate the physiological relevance of this transporter
514 within the heart. Another essential study conclusion is that using high doses of the SGLT

515 inhibitor phlorizin exerts a drastic effect on cardiac glucose transport, independent of SGLT1.
516 Therefore, extreme caution appears warranted when employing this inhibitor to investigate
517 SGLTs or, more specifically, the function of SGLT1.

518

519 **Acknowledgments**

520 We want to thank Jérôme Ambroise, Bertrand Bearzatto and Jean-Luc Gala for the precious

521 help in the performance and the analysis of RNA sequencing on mice.

522 **Grants**

523 This work was funded by grants from the *Fonds National de la Recherche Scientifique*

524 *(FNRS) et Médicale,* Belgium (T.0241.16, 2016–2018; T.0011.19, 2019–2020) and *Action de*

525 *Recherche Concertée de la Communauté Wallonie-Bruxelles,* Belgium (ARC 18/23-094).

526 LF was supported by the Fund for Scientific Research in Industry and Agriculture (FRIA); SH

527 is the research associate, and LB is the director of research of FNRS, Belgium.

528 **Disclosures**

529 This work was supported by unrestricted grants form Astra Zeneca.

530

References

1. **Abel ED**. Glucose transport in the heart. *Front Biosci* 9: 201-215, 2004.
2. **Balteau M, Van Steenbergen A, Timmermans AD, Dessy C, Behets-Wydemans G, Tajeddine N, Castanares-Zapatero D, Gilon P, Vanoverschelde JL, Horman S, Hue L, Bertrand L, and Beauloye C**. AMPK activation by glucagon-like peptide-1 prevents NADPH oxidase activation induced by hyperglycemia in adult cardiomyocytes. *Am J Physiol Heart Circ Physiol* 307: H1120-1133, 2014.
3. **Banerjee SK, McGaffin KR, Pastor-Soler NM, and Ahmad F**. SGLT1 is a novel cardiac glucose transporter that is perturbed in disease states. *Cardiovasc Res* 84: 111-118, 2009.
4. **Banerjee SK, Wang DW, Alzamora R, Huang XN, Pastor-Soler NM, Hallows KR, McGaffin KR, and Ahmad F**. SGLT1, a novel cardiac glucose transporter, mediates increased glucose uptake in PRKAG2 cardiomyopathy. *J Mol Cell Cardiol* 49: 683-692, 2010.
5. **Battault S, Renguet E, Van Steenbergen A, Horman S, Beauloye C, and Bertrand L**. Myocardial glucotoxicity: Mechanisms and potential therapeutic targets. *Arch Cardiovasc Dis* 113: 736-748, 2020.
6. **Berry GT, Wu S, Buccafusca R, Ren J, Gonzales LW, Ballard PL, Golden JA, Stevens MJ, and Greer JJ**. Loss of murine Na+/myo-inositol cotransporter leads to brain myo-inositol depletion and central apnea. *J Biol Chem* 278: 18297-18302, 2003.
7. **Bertrand L, Ginion A, Beauloye C, Hebert AD, Guigas B, Hue L, and Vanoverschelde JL**. AMPK activation restores the stimulation of glucose uptake in an in vitro model of insulin-resistant cardiomyocytes via the activation of protein kinase B. *Am J Physiol Heart Circ Physiol* 291: H239-250, 2006.
8. **Bhatt DL, Szarek M, Steg PG, Cannon CP, Leiter LA, McGuire DK, Lewis JB, Riddle MC, Voors AA, Metra M, Lund LH, Komajda M, Testani JM, Wilcox CS, Ponikowski P, Lopes RD, Verma S, Lapuerta P, Pitt B, and Investigators S-WT**. Sotagliflozin in Patients with Diabetes and Recent Worsening Heart Failure. *N Engl J Med* 2020.
9. **Bisignano P, Ghezzi C, Jo H, Polizzi NF, Althoff T, Kalyanaraman C, Friemann R, Jacobson MP, Wright EM, and Grabe M**. Inhibitor binding mode and allosteric regulation of Na(+)-glucose symporters. *Nat Commun* 9: 5245, 2018.
10. **Bontemps F, Hue L, and Hers HG**. Phosphorylation of glucose in isolated rat hepatocytes. Sigmoidal kinetics explained by the activity of glucokinase alone. *Biochem J* 174: 603-611, 1978.
11. **Chin KL, Ofori-Asenso R, Hopper I, von Lueder TG, Reid CM, Zoungas S, Wang BH, and Liew D**. Potential mechanisms underlying the cardiovascular benefits of sodium glucose cotransporter 2 inhibitors: a systematic review of data from preclinical studies. *Cardiovasc Res* 115: 266-276, 2019.
12. **Coady MJ, Wallendorff B, Gagnon DG, and Lapointe JY**. Identification of a novel Na+/myo-inositol cotransporter. *J Biol Chem* 277: 35219-35224, 2002.
13. **Crane RK**. Intestinal absorption of sugars. *Physiol Rev* 40: 789-825, 1960.
14. **Di Franco A, Cantini G, Tani A, Coppini R, Zecchi-Orlandini S, Raimondi L, Luconi M, and Mannucci E**. Sodium-dependent glucose transporters (SGLT) in human ischemic heart: A new potential pharmacological target. *Int J Cardiol* 243: 86-90, 2017.
15. **Ehrenkranz JR, Lewis NG, Kahn CR, and Roth J**. Phlorizin: a review. *Diabetes Metab Res Rev* 21: 31-38, 2005.
16. **Fueger BJ, Czernin J, Hildebrandt I, Tran C, Halpern BS, Stout D, Phelps ME, and Weber WA**. Impact of animal handling on the results of 18F-FDG PET studies in mice. *J Nucl Med* 47: 999-1006, 2006.
17. **Ghezzi C, Loo DDF, and Wright EM**. Physiology of renal glucose handling via SGLT1, SGLT2 and GLUT2. *Diabetologia* 61: 2087-2097, 2018.
18. **Ginion A, Auquier J, Benton CR, Mouton C, Vanoverschelde JL, Hue L, Horman S, Beauloye C, and Bertrand L**. Inhibition of the mTOR/p70S6K pathway is not involved in the insulin-sensitizing effect of AMPK on cardiac glucose uptake. *Am J Physiol Heart Circ Physiol* 301: H469-477, 2011.

19. **Gorboulev V, Schurmann A, Vallon V, Kipp H, Jaschke A, Klessen D, Friedrich A, Scherneck S, Rieg T, Cunard R, Veyhl-Wichmann M, Srinivasan A, Balen D, Breljak D, Rexhepaj R, Parker HE, Gribble FM, Reimann F, Lang F, Wiese S, Sabolic I, Sendtner M, and Koepsell H**. Na(+)-D-glucose cotransporter SGLT1 is pivotal for intestinal glucose absorption and glucose-dependent incretin secretion. *Diabetes* 61: 187-196, 2012.

20. **Grempler R, Augustin R, Froehner S, Hildebrandt T, Simon E, Mark M, and Eickelmann P**. Functional characterisation of human SGLT-5 as a novel kidney-specific sodium-dependent sugar transporter. *FEBS Lett* 586: 248-253, 2012.

21. **Han Y, Cho YE, Ayon R, Guo R, Youssef KD, Pan M, Dai A, Yuan JX, and Makino A**. SGLT inhibitors attenuate NO-dependent vascular relaxation in the pulmonary artery but not in the coronary artery. *Am J Physiol Lung Cell Mol Physiol* 309: L1027-1036, 2015.

22. **Huisman MC, Reder S, Weber AW, Ziegler SI, and Schwaiger M**. Performance evaluation of the Philips MOSAIC small animal PET scanner. *Eur J Nucl Med Mol Imaging* 34: 532-540, 2007.

23. **Kanwal A, Nizami HL, Mallapudi S, Putcha UK, Mohan GK, and Banerjee SK**. Inhibition of SGLT1 abrogates preconditioning-induced cardioprotection against ischemia-reperfusion injury. *Biochem Biophys Res Commun* 472: 392-398, 2016.

24. **Kashiwagi Y, Nagoshi T, Yoshino T, Tanaka TD, Ito K, Harada T, Takahashi H, Ikegami M, Anzawa R, and Yoshimura M**. Expression of SGLT1 in Human Hearts and Impairment of Cardiac Glucose Uptake by Phlorizin during Ischemia-Reperfusion Injury in Mice. *PLoS One* 10: e0130605, 2015.

25. **Kinne RK, and Castaneda F**. SGLT inhibitors as new therapeutic tools in the treatment of diabetes. *Handb Exp Pharmacol* 105-126, 2011.

26. **Landau BR, Spring-Robinson CL, Muzic RF, Jr., Rachdaoui N, Rubin D, Berridge MS, Schumann WC, Chandramouli V, Kern TS, and Ismail-Beigi F**. 6-Fluoro-6-deoxy-D-glucose as a tracer of glucose transport. *Am J Physiol Endocrinol Metab* 293: E237-245, 2007.

27. **Li Z, Agrawal V, Ramratnam M, Sharma RK, D'Auria S, Sincoular A, Jakubiak M, Music ML, Kutschke WJ, Huang XN, Gifford L, and Ahmad F**. Cardiac Sodium-Glucose Co-Transporter 1 (SGLT1) is a Novel Mediator of Ischemia/Reperfusion Injury. *Cardiovasc Res* 2019.

28. **Madunic IV, Breljak D, Karaica D, Koepsell H, and Sabolic I**. Expression profiling and immunolocalization of Na(+)-D-glucose-cotransporter 1 in mice employing knockout mice as specificity control indicate novel locations and differences between mice and rats. *Pflugers Arch* 469: 1545-1565, 2017.

29. **Matsushita N, Ishida N, Ibi M, Saito M, Sanbe A, Shimojo H, Suzuki S, Koepsell H, Takeishi Y, Morino Y, Taira E, Sawa Y, and Hirose M**. Chronic Pressure Overload Induces Cardiac Hypertrophy and Fibrosis via Increases in SGLT1 and IL-18 Gene Expression in Mice. *Int Heart J* 59: 1123-1133, 2018.

30. **Mueckler M, and Thorens B**. The SLC2 (GLUT) family of membrane transporters. *Mol Aspects Med* 34: 121-138, 2013.

31. **Murata H, Hruz PW, and Mueckler M**. Indinavir inhibits the glucose transporter isoform Glut4 at physiologic concentrations. *AIDS* 16: 859-863, 2002.

32. **Neal B, Perkovic V, Mahaffey KW, de Zeeuw D, Fulcher G, Erondu N, Shaw W, Law G, Desai M, Matthews DR, and Group CPC**. Canagliflozin and Cardiovascular and Renal Events in Type 2 Diabetes. *N Engl J Med* 377: 644-657, 2017.

33. **Panayotova-Heiermann M, Loo DDF, Kong C-T, Lever JE, and Wright EM**. Sugar Binding to Na/Glucose Cotransporters Is Determined by the Carboxyl-terminal Half of the Protein. *Journal of Biological Chemistry* 271: 10029-10034, 1996.

34. **Passonneau JV, and Lauderdale VR**. A comparison of three methods of glycogen measurement in tissues. *Anal Biochem* 60: 405-412, 1974.

35. **Pepin ME, Drakos S, Ha CM, Tristani-Firouzi M, Selzman CH, Fang JC, Wende AR, and Wever-Pinzon O**. DNA methylation reprograms cardiac metabolic gene expression in end-stage human heart failure. *Am J Physiol Heart Circ Physiol* 317: H674-H684, 2019.

631 36. **Ramratnam M, Sharma RK, D'Auria S, Lee SJ, Wang D, Huang XY, and Ahmad F**. Transgenic
632 knockdown of cardiac sodium/glucose cotransporter 1 (SGLT1) attenuates PRKAG2 cardiomyopathy,
633 whereas transgenic overexpression of cardiac SGLT1 causes pathologic hypertrophy and dysfunction
634 in mice. *J Am Heart Assoc* 3: 2014.
635 37. **Renguet E, Ginion A, Gelinas R, Bultot L, Auquier J, Robillard Frayne I, Daneault C,**
636 **Vanoverschelde JL, Des Rosiers C, Hue L, Horman S, Beauloye C, and Bertrand L**. Metabolism and
637 acetylation contribute to leucine-mediated inhibition of cardiac glucose uptake. *Am J Physiol Heart*
638 *Circ Physiol* 313: H432-H445, 2017.
639 38. **Sala-Rabanal M, Hirayama BA, Loo DD, Chaptal V, Abramson J, and Wright EM**. Bridging the
640 gap between structure and kinetics of human SGLT1. *Am J Physiol Cell Physiol* 302: C1293-1305,
641 2012.
642 39. **Schwenk RW, Dirkx E, Coumans WA, Bonen A, Klip A, Glatz JF, and Luiken JJ**. Requirement
643 for distinct vesicle-associated membrane proteins in insulin- and AMP-activated protein kinase
644 (AMPK)-induced translocation of GLUT4 and CD36 in cultured cardiomyocytes. *Diabetologia* 53:
645 2209-2219, 2010.
646 40. **Sims H, Smith KH, Bramlage P, and Minguet J**. Sotagliflozin: a dual sodium-glucose co-
647 transporter-1 and -2 inhibitor for the management of Type 1 and Type 2 diabetes mellitus. *Diabet*
648 *Med* 35: 1037-1048, 2018.
649 41. **Song P, Onishi A, Koepsell H, and Vallon V**. Sodium glucose cotransporter SGLT1 as a
650 therapeutic target in diabetes mellitus. *Expert Opin Ther Targets* 20: 1109-1125, 2016.
651 42. **Spurrell CH, Barozzi I, Mannion BJ, Blow MJ, Fukuda-Yuzawa Y, Afzal SY, Akiyama JA, Afzal**
652 **V, Tran S, Plajzer-Frick I, Novak CS, Kato M, Lee E, Garvin TH, Pham QT, Harrington AN, Lisgo S,**
653 **Bristow J, Cappola TP, Morley MP, Margulies KB, Pennacchio LA, Dickel DE, and Visel A**. 2019.
654 43. **Stanley W**. Regulation of energy substrate metabolism in the diabetic heart. *Cardiovascular*
655 *Research* 34: 25-33, 1997.
656 44. **Sweet ME, Cocciolo A, Slavov D, Jones KL, Sweet JR, Graw SL, Reece TB, Ambardekar AV,**
657 **Bristow MR, Mestroni L, and Taylor MRG**. Transcriptome analysis of human heart failure reveals
658 dysregulated cell adhesion in dilated cardiomyopathy and activated immune pathways in ischemic
659 heart failure. *BMC Genomics* 19: 812, 2018.
660 45. **Tabatabai NM, Blumenthal SS, Lewand DL, and Petering DH**. Differential regulation of
661 mouse kidney sodium-dependent transporters mRNA by cadmium. *Toxicol Appl Pharmacol* 177: 163-
662 173, 2001.
663 46. **Tazawa S, Yamato T, Fujikura H, Hiratochi M, Itoh F, Tomae M, Takemura Y, Maruyama H,**
664 **Sugiyama T, Wakamatsu A, Isogai T, and Isaji M**. SLC5A9/SGLT4, a new Na+-dependent glucose
665 transporter, is an essential transporter for mannose, 1,5-anhydro-D-glucitol, and fructose. *Life Sci* 76:
666 1039-1050, 2005.
667 47. **Van Steenbergen A, Balteau M, Ginion A, Ferte L, Battault S, Ravenstein CM, Balligand JL,**
668 **Daskalopoulos EP, Gilon P, Despa F, Despa S, Vanoverschelde JL, Horman S, Koepsell H, Berry G,**
669 **Hue L, Bertrand L, and Beauloye C**. Sodium-myoinositol cotransporter-1, SMIT1, mediates the
670 production of reactive oxygen species induced by hyperglycemia in the heart. *Sci Rep* 7: 41166, 2017.
671 48. **von Lewinski D, Gasser R, Rainer PP, Huber MS, Wilhelm B, Roessl U, Haas T, Wasler A,**
672 **Grimm M, Bisping E, and Pieske B**. Functional effects of glucose transporters in human ventricular
673 myocardium. *Eur J Heart Fail* 12: 106-113, 2010.
674 49. **von Lewinski D, Rainer PP, Gasser R, Huber MS, Khafaga M, Wilhelm B, Haas T, Machler H,**
675 **Rossl U, and Pieske B**. Glucose-transporter-mediated positive inotropic effects in human
676 myocardium of diabetic and nondiabetic patients. *Metabolism* 59: 1020-1028, 2010.
677 50. **Voss AA, Diez-Sampedro A, Hirayama BA, Loo DD, and Wright EM**. Imino sugars are potent
678 agonists of the human glucose sensor SGLT3. *Mol Pharmacol* 71: 628-634, 2007.
679 51. **Vrhovac I, Balen Eror D, Klessen D, Burger C, Breljak D, Kraus O, Radovic N, Jadrijevic S,**
680 **Aleksic I, Walles T, Sauvant C, Sabolic I, and Koepsell H**. Localizations of Na(+)-D-glucose
681 cotransporters SGLT1 and SGLT2 in human kidney and of SGLT1 in human small intestine, liver, lung,
682 and heart. *Pflugers Arch* 467: 1881-1898, 2015.

683 52. **White LW, and Landau BR**. Sugar Transport and Fructose Metabolism in Human Intestine in
684 Vitro. *J Clin Invest* 44: 1200-1213, 1965.
685 53. **Wiviott SD, Raz I, Bonaca MP, Mosenzon O, Kato ET, Cahn A, Silverman MG, Zelniker TA,**
686 **Kuder JF, Murphy SA, Bhatt DL, Leiter LA, McGuire DK, Wilding JPH, Ruff CT, Gause-Nilsson IAM,**
687 **Fredriksson M, Johansson PA, Langkilde AM, Sabatine MS, and Investigators D-T**. Dapagliflozin and
688 Cardiovascular Outcomes in Type 2 Diabetes. *N Engl J Med* 380: 347-357, 2019.
689 54. **Wong KP, Sha W, Zhang X, and Huang SC**. Effects of administration route, dietary condition,
690 and blood glucose level on kinetics and uptake of 18F-FDG in mice. *J Nucl Med* 52: 800-807, 2011.
691 55. **Wright EM, Loo DD, and Hirayama BA**. Biology of human sodium glucose transporters.
692 *Physiol Rev* 91: 733-794, 2011.
693 56. **Wright EM, Loo DD, Hirayama BA, and Turk E**. Surprising versatility of Na+-glucose
694 cotransporters: SLC5. *Physiology (Bethesda)* 19: 370-376, 2004.
695 57. **Yoshii A, Nagoshi T, Kashiwagi Y, Kimura H, Tanaka Y, Oi Y, Ito K, Yoshino T, Tanaka TD, and**
696 **Yoshimura M**. Cardiac ischemia-reperfusion injury under insulin-resistant conditions: SGLT1 but not
697 SGLT2 plays a compensatory protective role in diet-induced obesity. *Cardiovasc Diabetol* 18: 85,
698 2019.
699 58. **Zhao F-Q, and Keating A**. Functional Properties and Genomics of Glucose Transporters.
700 *Current Genomics* 8: 113-128, 2007.
701 59. **Zhou L, Cryan EV, D'Andrea MR, Belkowski S, Conway BR, and Demarest KT**. Human
702 cardiomyocytes express high level of Na+/glucose cotransporter 1 (SGLT1). *J Cell Biochem* 90: 339-
703 346, 2003.
704 60. **Zhu Y, Pereira RO, O'Neill BT, Riehle C, Ilkun O, Wende AR, Rawlings TA, Zhang YC, Zhang Q,**
705 **Klip A, Shiojima I, Walsh K, and Abel ED**. Cardiac PI3K-Akt impairs insulin-stimulated glucose uptake
706 independent of mTORC1 and GLUT4 translocation. *Mol Endocrinol* 27: 172-184, 2013.
707 61. **Zinman B, Wanner C, Lachin JM, Fitchett D, Bluhmki E, Hantel S, Mattheus M, Devins T,**
708 **Johansen OE, Woerle HJ, Broedl UC, Inzucchi SE, and Investigators E-RO**. Empagliflozin,
709 Cardiovascular Outcomes, and Mortality in Type 2 Diabetes. *N Engl J Med* 373: 2117-2128, 2015.

710

Figure legends

Figure 1. Cardiac glucose uptake in SGLT1 WT and $^{\Delta ex1}$KO mice. Glucose uptake in cardiomyocytes isolated from SGLT1 WT (n=6) and $^{\Delta ex1}$KO (n=6) animals was measured under normoglycemia (NG, 5mM), hyperglycemia (two hours, 21mM), and after insulin stimulation (30 min, 3nM). Two radioactive analogues were used: [^{3}H]-2-deoxyglucose (A) and [2-^{3}H]-glucose (B). (C) Glucose uptake was measured in isolated cardiomyocytes from SGLT1 WT (n=6) and $^{\Delta ex1}$KO (n=6) mice after insulin stimulation (30 min, 3nM) or oligomycin (one hour, 1μM) stimulation. In this experiment, the contribution of GLUT4 to glucose uptake under insulin or oligomycin was further evaluated in presence of indinavir (50μM, 30 min), used as a specific GLUT4 inhibitor. (D) Insulin-stimulated cardiac glucose uptake (SUV_{max}) was assessed *in vivo* in SGLT1 WT (n=8) and $^{\Delta ex1}$KO (n=7) animals using a PET scan. Glycemia measured at the end of experiment were for SGLT1 WT: control, 137±9mg/dl; insulin, 38±5*mg/dl with insulin and for SGLT1 $^{\Delta ex1}$KO: control, 164±10mg/dl; insulin, 41±4*mg/dl. (E) Glycogen content was evaluated in SGLT1 $^{\Delta ex1}$KO (n=9) and WT (n=8) total hearts. Data were expressed as means ± SEM. Statistical analysis was conducted via a two-way ANOVA (A–D) or t-test (E). * Indicates values statistically different from corresponding control, $p<0.05$; $ Indicates values statistically different from insulin alone, $p<0.05$. # Indicates values statistically different from oligomycin alone, $p<0.05$.

Figure 2. GLUT transporter expression and signalings in hearts from SGLT1 WT and $^{\Delta ex1}$KO mice. GLUT1 (A) and GLUT4 (B) mRNA was determined in SGLT1 WT (n=8) and $^{\Delta ex1}$KO (n=8) total hearts by RT-qPCR. Protein contents of GLUT1 (C) and GLUT4 (D) was assessed by immunoblotting in SGLT1 WT (n=8) and $^{\Delta ex1}$KO (n=7–8) total heart lysates. Immunoblots in (C) and (D) present 2 examples of both groups. Phosphorylations of Akt/PKB (E) and S6 (F) were analyzed by immunoblotting in SGLT1 WT (n=3) and $^{\Delta ex1}$KO (n=3) cardiomyocytes treated with hyperglycemia (two hours, 21 mM) or insulin (30 min, 3 nM).

(G) AMPK phosphorylation was assessed by immunoblotting on SGLT1 WT (n=6) and $^{\Delta ex1}$KO (n=6) cardiomyocytes treated with oligomycin (one hour, 1µM). Data were expressed as means ± SEM. Statistical analysis was performed via a t-test (A-D) or one-way ANOVA (E-G). * Indicates values statistically different from corresponding control, $p<0.05$.

Figure 3. Impact of phlorizin on cardiac glucose uptake *in vitro* and *in vivo* on SGLT1 WT and $^{\Delta ex1}$KO animals. (A) Influence of increasing concentrations of phlorizin on basal glucose uptake was measured in cardiomyocytes isolated from SGLT1 WT (n=7) and $^{\Delta ex1}$KO (n=6) mice using [2-^{3}H]-glucose as a radiotracer. Increasing concentrations of phlorizin were added to insulin stimulation, and glucose uptake was assessed with [2-^{3}H]-glucose in cardiomyocytes isolated from SGLT1 WT (n=7) and $^{\Delta ex1}$KO (n=6). A comparison of control and insulin-stimulated (30 min, 3nM) conditions was performed at three concentrations of phlorizin (45 min): 10µM, 100µM, and 1mM. Data were expressed as means ± SEM. Statistical analysis was carried out via a two-way ANOVA. * Indicates values statistically different from control, without insulin, $p<0.05$. $ Indicates values statistically different from corresponding control, insulin without phlorizin, $p<0.05$. (B) *In vivo* cardiac glucose uptake (SUV_{max}) was measured by a micro-PET scan in SGLT1 WT (n=5) and $^{\Delta ex1}$KO (n=4) animals treated with insulin (0.5U/kg) along with phlorizin (400mg/kg). Glycemia, measured at baseline and at the end the experiment, 2 h after insulin stimulation, are presented below the corresponding pictures. Data were expressed as means ± SEM. Statistical analysis was carried out via a two-way ANOVA. * Indicates values statistically different from corresponding control, insulin without phlorizin, $p<0.05$. # Indicates values statistically different from baseline, $p<0.05$.

Figure 4. Impact of phlorizin at higher concentration on insulin signaling. The effect of 1mM of phlorizin on Akt/PKB (A) and S6 (B) phosphorylation was evaluated by immunoblotting in SGLT1 WT (n=5–6) and $^{\Delta ex1}$KO (n=5–6) cardiomyocytes. (C) Akt/PKB

761 phosphorylation was assessed by immunoblotting in hearts from SGLT1 WT (n=5) mice
762 treated with insulin (0.5U/kg) along with phlorizin (400mg/kg). Data were expressed as
763 means ± SEM. Statistical analysis was carried out via a two-way ANOVA. * Indicates values
764 statistically different from corresponding control, without treatment, $p<0.05$. # Indicates
765 values statistically different from corresponding control, phlorizin without insulin, $p<0.05$. $
766 Indicates values statistically different from insulin without phlorizin, $p<0.05$.

767 **Figure 5. Impact of phlorizin at higher concentration on GLUT4 translocation**. GLUT4
768 translocation was analyzed in adult rat cardiomyocytes (n=4) treated with 1mM phlorizin (45
769 min) or 3nM insulin (30 min). The scale of these pictures represents 50µm. Data were
770 expressed as means ± SEM. Statistical analysis was performed via a two-way ANOVA. #
771 Indicates values statistically different from control, phlorizin without insulin, $p<0.05$.

772 **Figure 6. Mouse slc5a1 transcripts in WT and $^{\Delta ex1}$KO hearts.** (A) Genomic DNA has been
773 extracted from SGLT1 WT and $^{\Delta ex1}$KO hearts and genotyping was performed as described
774 elsewhere (19). (B) SGLT1 mRNA exons and coding sequence (CDS) are represented.
775 Amplifications of exon 1-exon 15 (C), exon 8-exon 15 (D) and exon 9-exon 15 (E) were
776 performed by PCR in SGLT1 WT and $^{\Delta ex1}$KO hearts and intestines as well as cardiomyocytes
777 isolated from C57BL/6N. Results of amplification of the other exons of SGLT1 are resumed
778 in Supplementary Fig. 1. (F) Data from RNA seq on SMIT1 WT and KO cardiac mRNA were
779 aligned with SGLT1 sequence. Each blue bar represent a read matching SGLT1 sequence and
780 dotted bars indicate beginning of exon 9. Three representative mice are represented.

781 **Figure 7. SLC5A1 transcripts found in human hearts.** (A-B) Representation of SLC5A1
782 variants in human. Variant A (A) and variant B (B) amplifications were performed in human
783 hearts with the help of specific primers deciphering between the two isoforms. (C-D) Data
784 from RNA seq of human hearts from three independent studies; Study 1 (44), Study 2 (42)
785 and Study 3 (35); were aligned with sequence of SLC5A1 variant A (C) or variant B (D).

Dotted bars indicate beginning of the common sequence between the two variants. One representative heart of each study is represented.

Figure 8. Putative SGLT1 proteins expressed in the heart. (A) Schematic structure of SGLT1 protein is represented and main residues involved in glucose and sodium bindings are highlighted in red, adapted from (55). (B-C) Representation of the hypothetical truncated SGLT1 proteins expressed in mouse (B) and human (C) hearts.

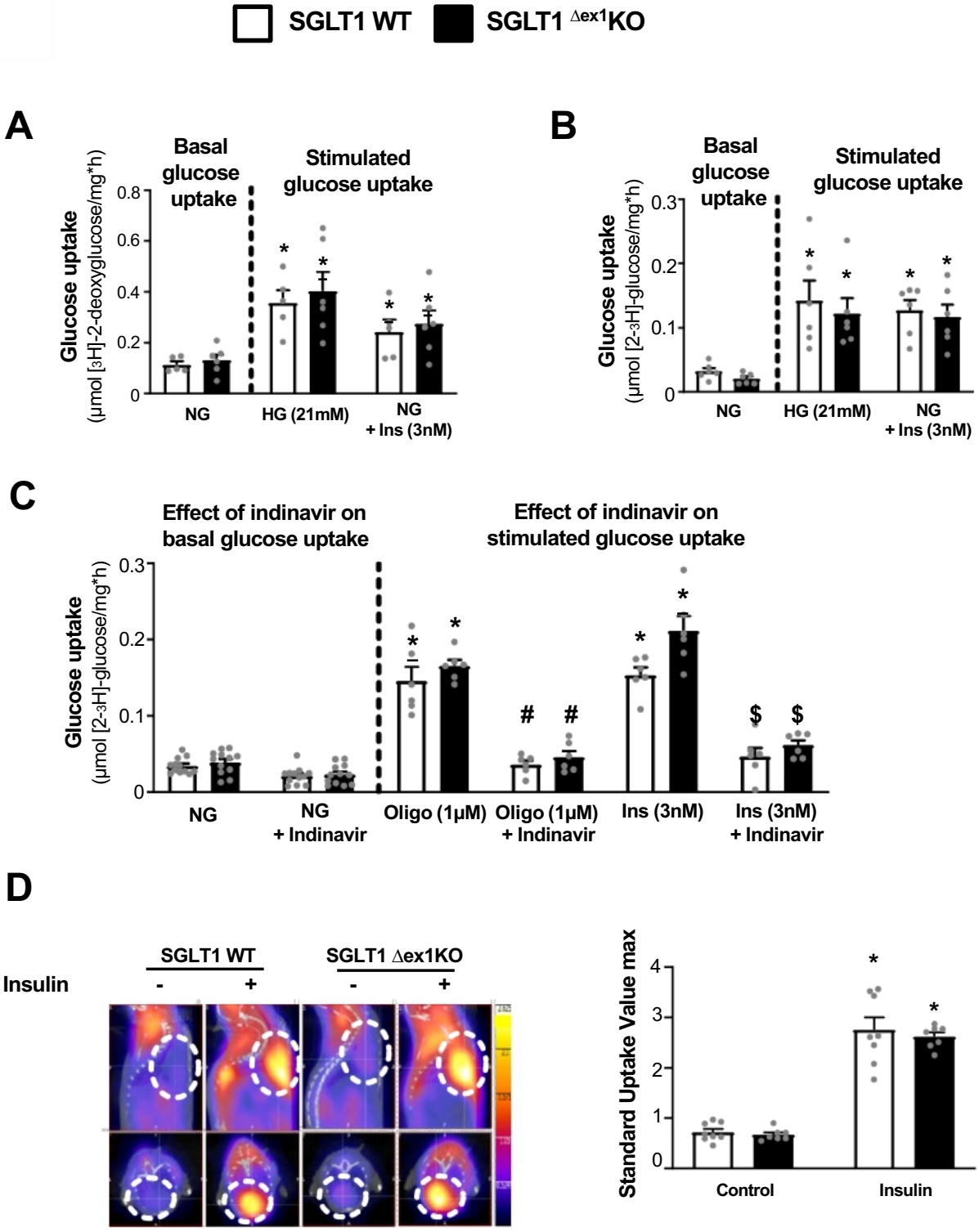

Fig. 1.

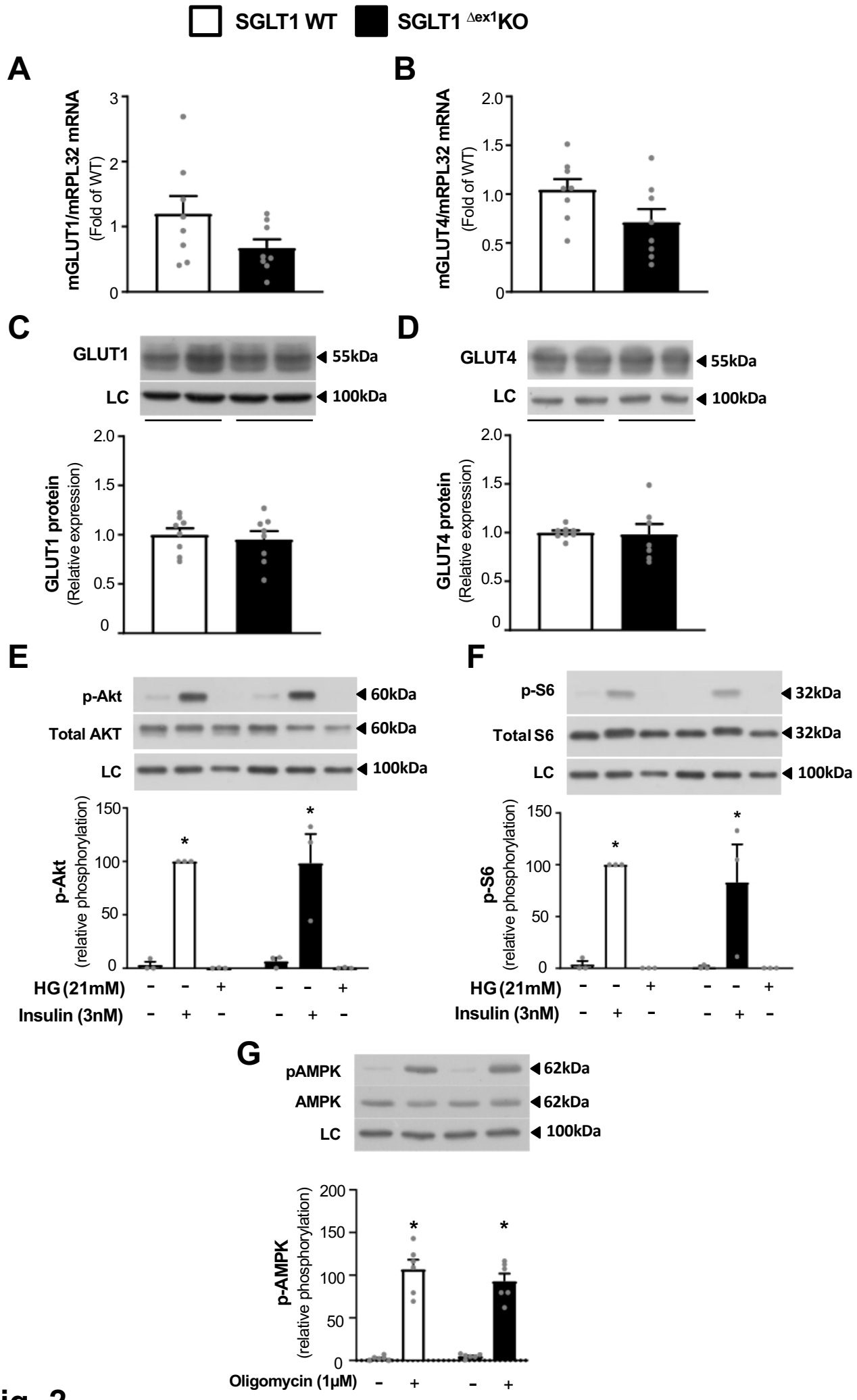

Fig. 2.

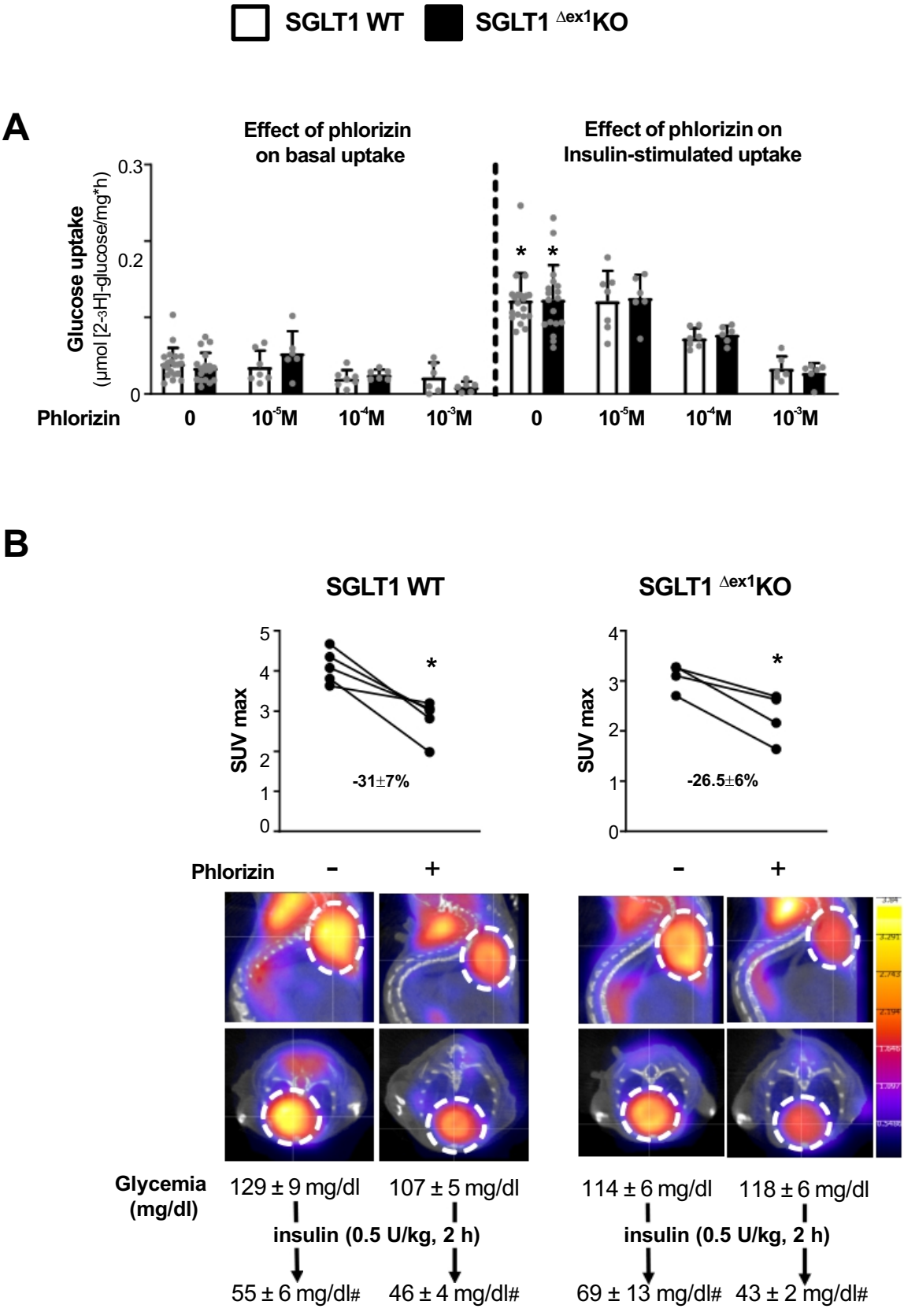

Fig. 3.

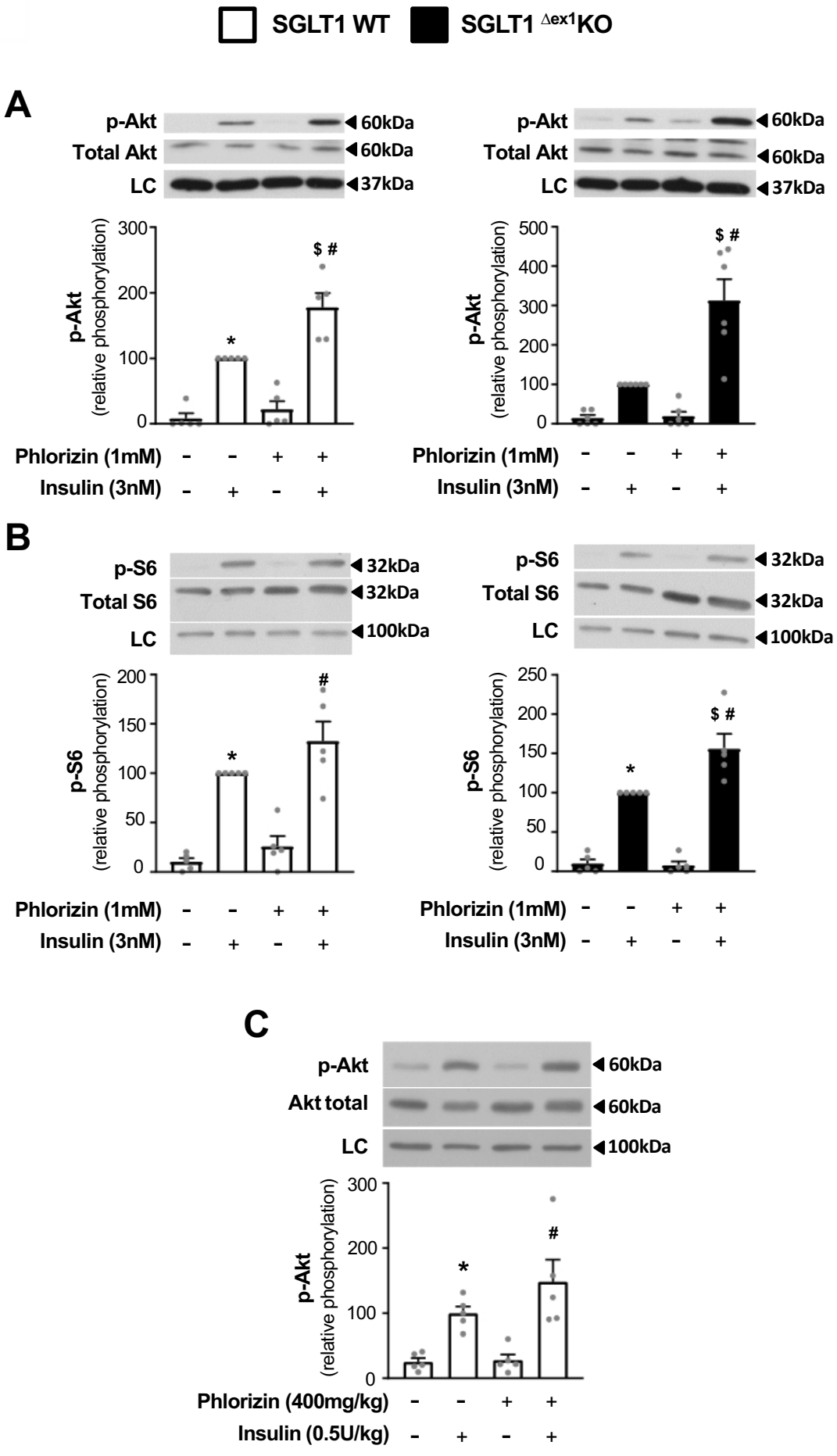

Fig. 4.

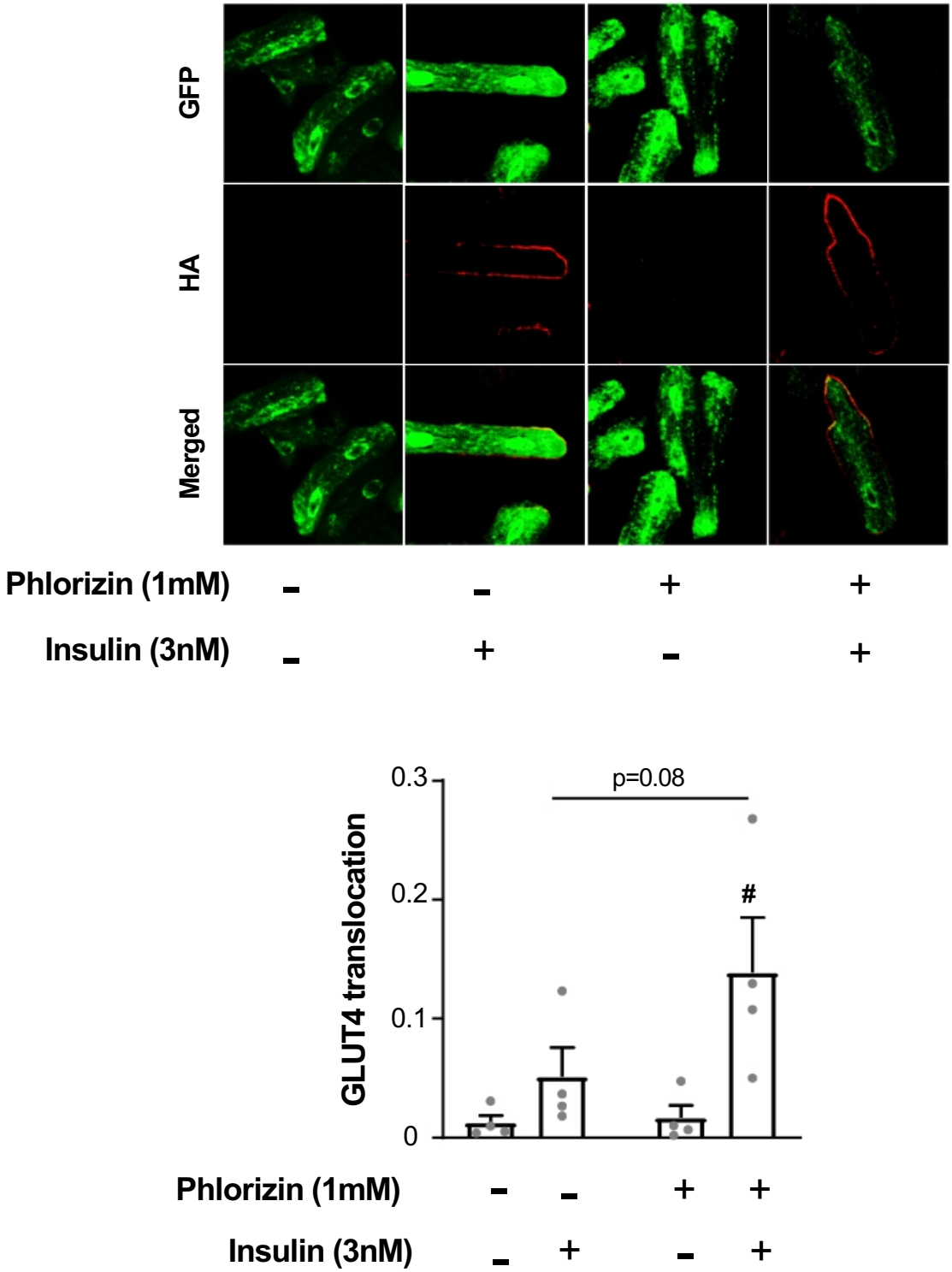

Fig. 5.

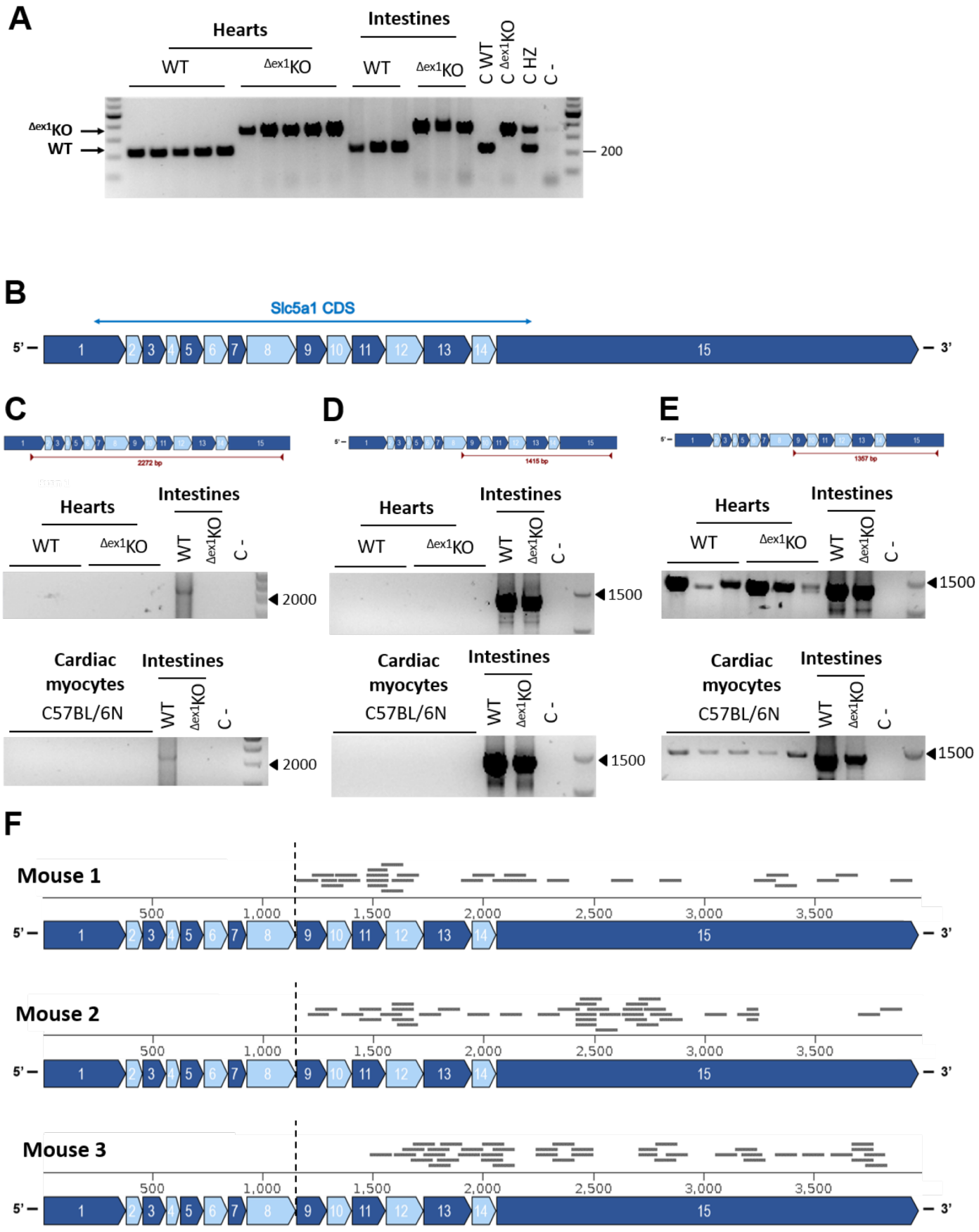

Fig. 6.

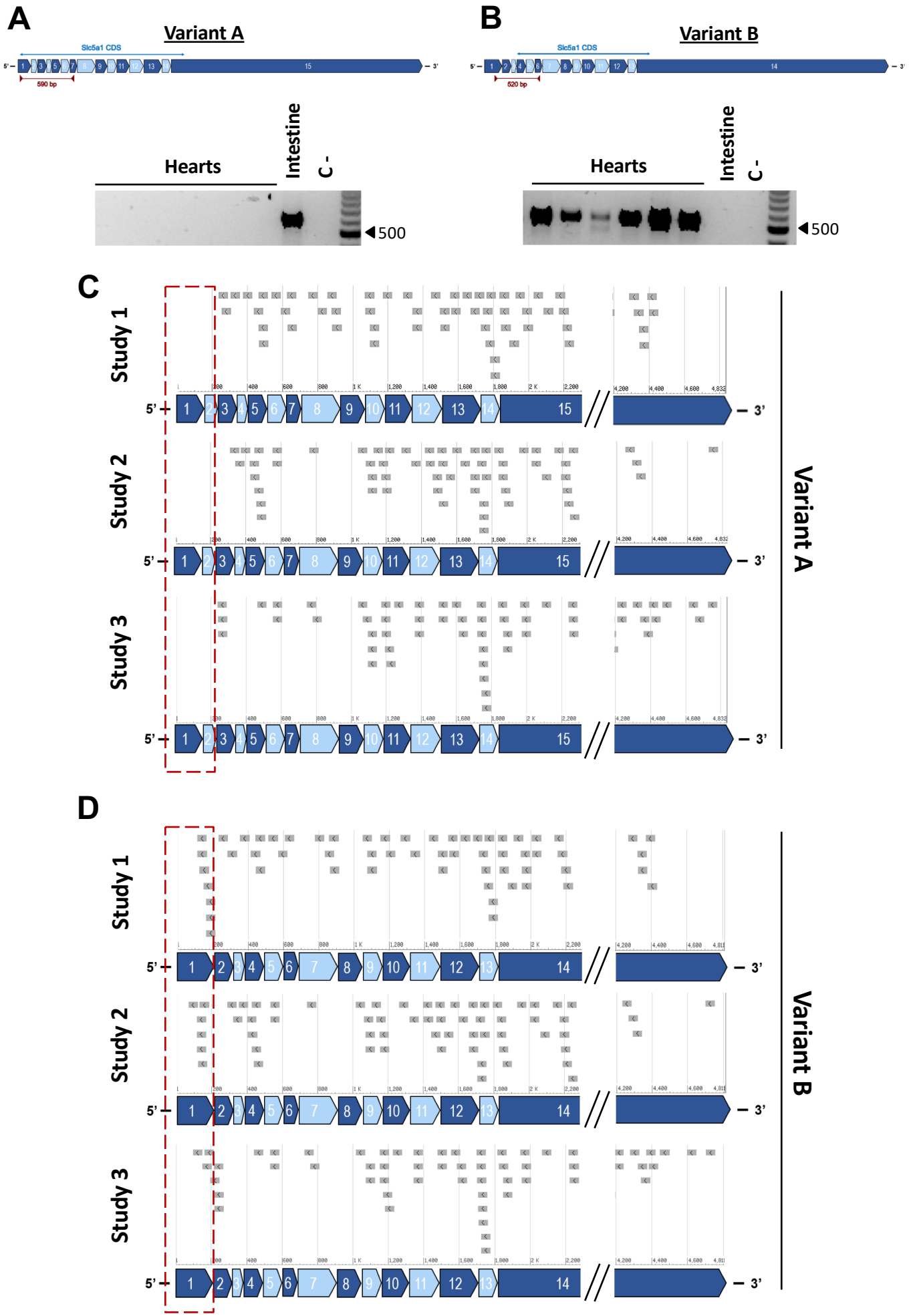

Fig. 7.

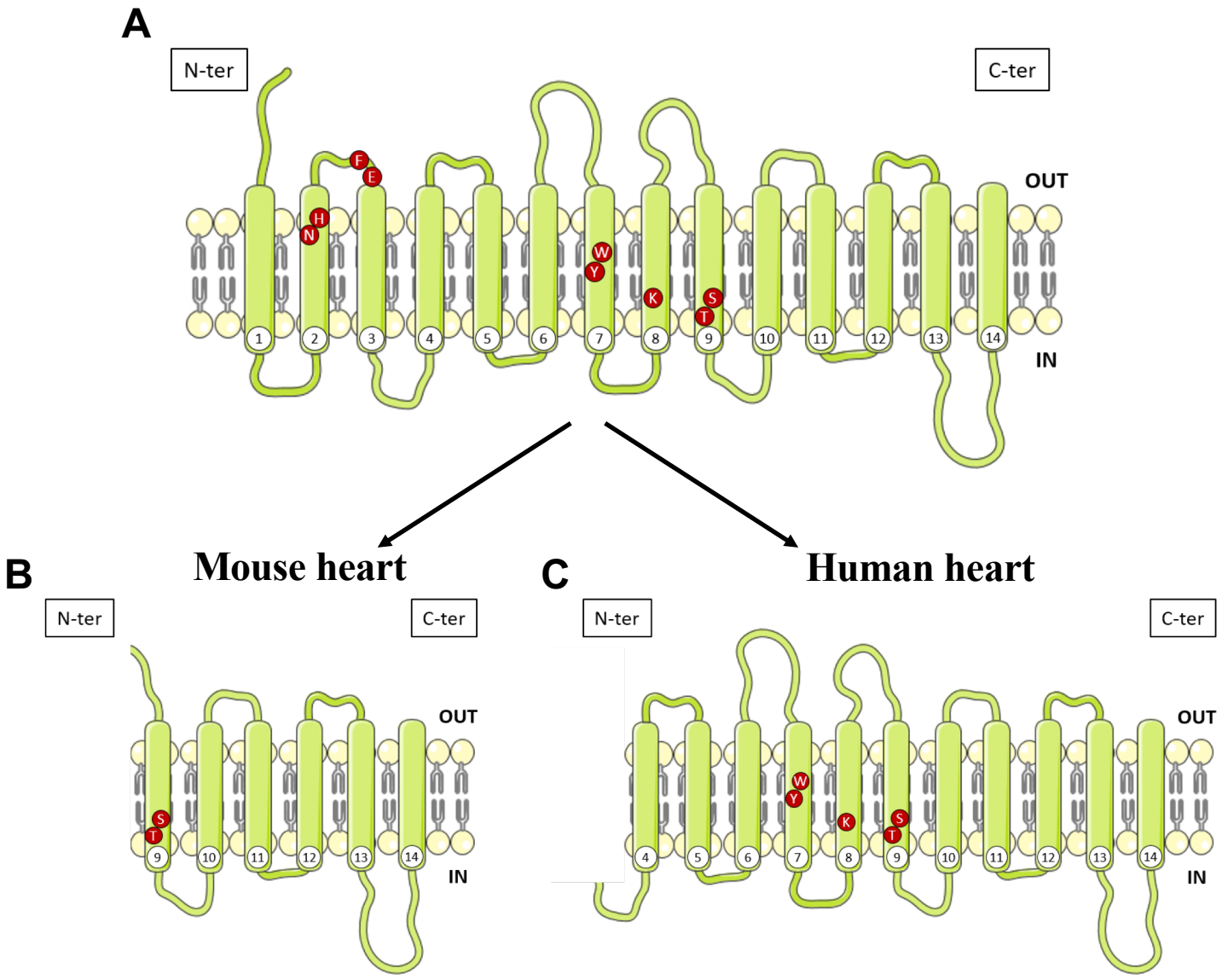

Fig. 8.